machines

MDPI

Article

AdaptiveBackstepping Control of an Unmanned Aerial Manipulator

Muhammad Awais Rafique, Mohssen E. Elshaar and Alan F. Lynch *

Department of Electrical and Computer Engineering, University of Alberta, Edmonton, AB T6G 1H9, Canada; mrafique@ualberta.ca (M.A.R.); elshaar@ualberta.ca (M.E.E.)
* Correspondence: alynch@ualberta.ca

Abstract

This paper presents an adaptive backstepping feedback control design for an unmanned aerial manipulator (UAM) that consists of an unmanned aerial vehicle (UAV) with an attached robotic arm. The effect of the arm is treated as a disturbance force and torque, as well as a parametric uncertainty in inertial parameters. The proposed adaptive law guarantees disturbance rejection assuming constant parameters and disturbances. In practice, this assumption includes the case of fixed-arm configurations. To validate the control design, numerical simulations are performed, including a realistic pick-and-place scenario.

Keywords: unmanned aerial vehicle (UAV); unmanned aerial manipulation (UAM); motion control; stability analysis

1. Introduction

Research on unmanned aerial vehicles (UAVs) is currently focused on expanding their capabilities for aerial manipulation. Such manipulation tasks span a wide range of applications, including payload transport [1] and non-destructive infrastructure testing [2]. Normally, aerial manipulation platforms involve some form of "arm" mounted to a UAV, typically a multirotor. The combined UAV/arm system is referred to as an unmanned aerial manipulator (UAM). Research on UAMs is currently very active, and a summary of results to date can be found in [3,4]. This paper considers a UAM consisting of a traditional underactuated multirotor UAV and two-DoF (Degree of Freedom) manipulator arm with a payload end-effector. We consider the problem of free motion control of the UAM and directly compensate for the effect of the arm's influence. Applications include payload transport, and a pick-and-place simulation is included in this paper.

As manipulation can involve contact with the environment, some of the existing work investigates the simultaneous control of contact force and motion. Early examples of that work for a UAV with a single fixed single-link arm include [5–7], and more advanced work can be found in [3,4]. However, since this paper focuses on free motion control, we review existing work on that topic. We also consider work on the more complex case of multi-DoF arms. Pure motion control for multi-DoF arm UAMs can be divided into two approaches: (i) decentralized control of the UAV and arm [8–15] and (ii) centralized control of the entire UAM system [16–22]. The first approach generally benefits from simpler controllers, but coupling disturbances are often neglected, leading to an incomplete closed-loop analysis. The second approach normally accounts for arm/UAV coupling but can lead to complex controllers. This paper adopts the first approach by controlling the UAV center of mass

check for updates

Academic Editor: Tao Li

Received: 26 August 2025
Revised: 27 September 2025
Accepted: 30 September 2025
Published: 4 October 2025

Citation: Rafique, M.A.; Elshaar, M.E.; Lynch, A.F. Adaptive Backstepping Control of an Unmanned Aerial Manipulator. *Machines* **2025**, *13*, 915. https://doi.org/10.3390/machines13100915

Copyright: © 2025 by the authors. Licensee MDPI, Basel, Switzerland. This article is an open access article distributed under the terms and conditions of the Creative Commons Attribution (CC BY) license (https://creativecommons.org/licenses/by/4.0/).

(CoM) position and yaw while compensating for the effect of the arm by introducing uncertain inertial parameters and force/torque disturbances.

An example of Approach (i) includes [8], which considers a hexrotor UAV with a four-DoF arm. A disturbance observer-based design from [23] is used to control the UAV attitude dynamics. The outer loop is controlled without accounting for subsystem coupling. The work in [24] only considers the control of the outer loop using a model reference control approach. UAV mass is taken as the unknown parameter. The effect of coupling forces and torques due to the arm is not considered. In [25], arm joint states are explicitly estimated with an observer to compute disturbance torque, which are then compensated for in a quaternion-based attitude controller. More recently, ref. [26] proposed an adaptive incremental nonlinear dynamic inversion scheme, where a Kalman filter updates the control effectiveness matrix to account for arm-induced parameter variation. In contrast to the above-mentioned designs, our approach avoids arm state reconstruction, models the arm's influence as parametric uncertainties and external disturbances, and proposes an adaptive backstepping design to guarantee UAM position and yaw trajectory tracking. We remark that the literature on robust control for bare UAVs, i.e., without an arm, is related to Approach (i), for example, disturbance rejection methods [27,28] and fractional-order sliding-mode backstepping for finite-time quadcopter stabilization [29]. Furthermore, decentralized control of slung load systems is also related to UAM motion control as the slung load is normally modeled as an unactuated two-rotational-DoF "arm" [1].

In this paper, our objective is trajectory tracking of the UAV CoM and yaw. The effect of the arm on the UAV is modeled in two ways: it adds a force and torque disturbance to the UAV and introduces parametric uncertainty e.g., arm motion alters the UAV CoM and inertia matrix. We are inspired by the work of [30,31] on bare UAV motion control. These contributions only consider force and torque disturbances, while all inertial parameters are assumed to be known. Other adaptive schemes for bare UAVs that address parametric uncertainty in inertia and mass include [32]. However, that work does not account for the disturbance wrench.

This paper is organized as follows. Section 2 presents the model of the UAM. Section 3 presents model assumptions, formulates the control problem, proposes a control design, and performs stability analysis. Numerical simulations are presented in Section 4. Finally, Section 5 concludes the paper. The proposed control is based on the first author's thesis [33].

2. Modeling

Consider a UAM consisting of a UAV with an attached robotic arm. In this section, we present the UAV model and introduce force/torque disturbances and parametric uncertainties to model the effect of the arm. The UAV model neglects the effects of motor dynamics, rotor drag, and the rotor gyroscopic effects. The details on modeling these higher-order effects are discussed in [34,35].

Consider Figure 1. Let $\mathcal{N}$ denote an inertial navigation frame with basis vectors $\{n_1, n_2, n_3\}$ pointing north, east, and down, respectively. Let $\mathcal{B}$ denote a body-fixed frame whose origin coincides with the UAV center of mass (CoM). The basis vectors of $\mathcal{B}$ are $\{b_1, b_2, b_3\}$, pointing forward, right, and downward relative to the UAV. The position of the origin of $\mathcal{B}$ relative to the origin of $\mathcal{N}$ is denoted as $p \in \mathbb{R}$, which is expressed in $\mathcal{N}$. The linear velocity of the UAV CoM is denoted as $v = \dot{p} \in \mathbb{R}$. The orientation of $\mathcal{B}$ relative to $\mathcal{N}$ is described by rotation matrix $R \in \mathrm{SO}(3)$. The angular velocity of the UAV relative to $\mathcal{N}$ expressed in $\mathcal{B}$ is denoted as $\omega \in \mathbb{R}^3$ and the rotational kinematics is

$$\dot{R} = R\mathrm{S}(\omega), \tag{1}$$

where

$$\mathrm{S}(x) = \begin{bmatrix} 0 & -x_3 & x_2 \\ x_3 & 0 & -x_1 \\ -x_2 & x_1 & 0 \end{bmatrix}, \qquad x = \begin{bmatrix} x_1 \\ x_2 \\ x_3 \end{bmatrix} \in \mathbb{R}^3.$$

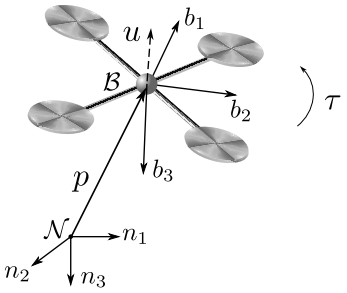


Figure 1. Quadrotor modeling notation.

The UAV input is total propeller thrust $u \geq 0$, which creates a force in the $-b_3$ direction, and torque $\tau \in \mathbb{R}^3$ on $\mathcal{B}$. Letting m denote UAV mass and $J \in \mathbb{R}^{3\times 3}$ denote UAV inertia, the UAV dynamics are

$$\begin{aligned} m\dot{v} &= mg_3 - F, \\ J\dot{\omega} &= -\mathrm{S}(\omega)J\omega + \tau \end{aligned} \tag{2}$$

where $F = -uR_3$, $R_3 = Re_3, e_3 = [0,0,1]^\top$, and $g_3 = ge_3$ is gravitational acceleration. We remark that (2) models the UAV in isolation from the arm. To account for the effect of the arm, we introduce disturbance force $d_f \in \mathbb{R}^3$ and torque $d_\tau \in \mathbb{R}^3$. Further, we consider inertial parameters $a \in \mathbb{R}$ and J as uncertain. Hence, the UAM model is taken as

$$\dot{p} = v, \tag{3a}$$
$$\dot{v} = g_3 - auR_3 + d_f, \tag{3b}$$
$$\dot{R} = R\mathrm{S}(\omega), \tag{3c}$$
$$J\dot{\omega} = -\mathrm{S}(\omega)J\omega + \tau + d_\tau. \tag{3d}$$

Further details on using (3) to model the UAM are given in [33] (Sections 2.2.4 and 2.2.5).

Note that J in (3) is a positive definite symmetric matrix with six unique entries. These entries of J define the vector $J_v = [J_{xx}, J_{yy}, J_{zz}, J_{xy}, J_{yz}, J_{zx}]^\top \in \mathbb{R}^6$. Using J_v we can re-write the $\mathrm{S}(\omega)J\omega$ term in (3d) as

$$\mathrm{S}(\omega)J\omega = \Phi(\omega)J_v, \tag{4}$$

where

$$\Phi(\omega) = \begin{bmatrix} 0 & -\omega_2\omega_3 & \omega_2\omega_3 & -\omega_1\omega_3 & \omega_2^2 - \omega_3^2 & \omega_1\omega_2 \\ \omega_1\omega_3 & 0 & -\omega_1\omega_3 & \omega_2\omega_3 & -\omega_1\omega_2 & \omega_3^2 - \omega_1^2 \\ -\omega_1\omega_2 & \omega_1\omega_2 & 0 & \omega_1^2 - \omega_2^2 & \omega_1\omega_3 & -\omega_2\omega_3 \end{bmatrix}.$$

In model (3) we take a, J_v, d_f and d_τ as unknown constants and denote $\hat{a} \in \mathbb{R} > 0$, $\hat{J}_v \in \mathbb{R}^6$, $\hat{d}_f \in \mathbb{R}^3$, and $\hat{d}_\tau \in \mathbb{R}^3$ as their estimates. Estimation errors are defined as $\tilde{a} = a - \hat{a}$, $\tilde{J}_v = J_v - \hat{J}_v$, $\tilde{d}_f = d_f - \hat{d}_f$, and $\tilde{d}_\tau = d_\tau - \hat{d}_\tau$.

3. Control Design

This section presents the control design for the UAM model (3). Figure 2 shows the structure of the proposed control, where the arm is controlled separately using PID control. In this figure, we denote α as the arm's joint angles and their desired reference as α_d. The proposed control compensates for the effect of the arm using an adaptive backstepping

design method. The control objective is trajectory tracking for UAV CoM position p and UAV heading ψ. We first present the design for tracking p and then extend it for tracking ψ.

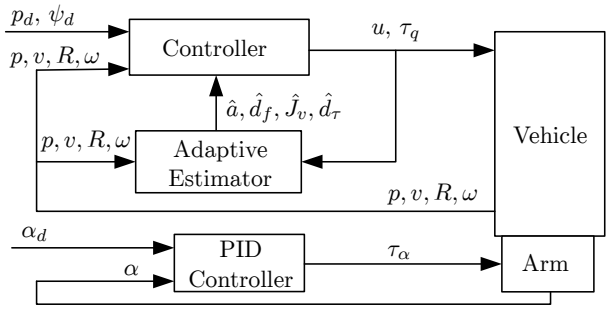


Figure 2. The proposed UAM controller structure. The control of the UAV and that of the arm are decoupled.

3.1. Position Tracking Control

The backstepping methodology performs tracking error stabilization design iteratively and subsystem-at-a-time by defining a virtual control input at each stage and using a control Lyapunov function (CLF) design procedure. In particular, we begin with the position dynamics subsystem (3a) and treat v as the virtual input to stabilize position tracking error $z_1 = p - p_d \in \mathbb{R}^3$, where p_d denotes the desired position reference. As v is not a physical input and cannot be directly controlled, the next iteration of backstepping stabilizes an error state $z_2 \in \mathbb{R}^3$, which includes the error between the virtual input and actual velocity v. This stabilization design is achieved with a CLF treating linear acceleration as an input. Unlike the first stage of the design, now the state feedback depends on unknown parameters a and d_f. This introduces parameter error terms that are compensated for adaptively at a later stage of the design. Ultimately, a key benefit of the method is that it formally accounts for uncertainty to achieve asymptotic tracking for position and yaw. Ultimately, parameters are not required to converge to their actual values, but rather, they are used to ensure position and yaw tracking occurs.

We begin the backstepping procedure by taking the time derivative of position error:

$$\dot{z}_1 = \dot{p} - \dot{p}_d = v - v_d, \tag{5}$$

where $v_d = \dot{p}_d \in \mathbb{R}^3$ denotes the desired linear velocity. In order to stabilize these dynamics, consider the Lyapunov function $V_1 = \frac{1}{2} z_1^\top z_1$. Taking its time derivative gives

$$\begin{aligned} \dot{V}_1 &= z_1^\top \dot{z}_1 \\ &= z_1^\top (v - v_d). \qquad \text{(from (5))} \end{aligned}$$

Adding and subtracting $k_1 z_1^\top z_1$ to $\dot{V}_1$, where $k_1 > 0$ is the controller gain, we obtain

$$\dot{V}_1 = -k_1 \|z_1\|^2 + z_1^\top (v - v_d + k_1 z_1). \tag{6}$$

From (6) we define the error variable $z_2 = v - v_d + k_1 z_1$, so we can express (5) as

$$\dot{z}_1 = -k_1 z_1 + z_2. \tag{7}$$

Now we move to the second stage of the backstepping design where we stabilize z_2. We first take the time derivative of z_2, and substituting (7) and the linear velocity dynamics (3b), we obtain

$$\dot{z}_2 = g_3 - auR_3 + d_f - \dot{v}_d - k_1^2 z_1 + k_1 z_2.$$

Using $a = \hat{a} + \tilde{a}$, and $d_f = \hat{d}_f + \tilde{d}_f$, we obtain

$$\dot{z}_2 = g_3 - \hat{a}uR_3 + \hat{d}_f - \dot{v}_d - k_1^2 z_1 + k_1 z_2 - \tilde{a}uR_3 + \tilde{d}_f. \tag{8}$$

For (8) we consider the Lyapunov function $V_2 = V_1 + \frac{1}{2} z_2^\top z_2$, whose time derivative is

$$\dot{V}_2 = \dot{V}_1 + z_2^\top \dot{z}_2. \tag{9}$$

Substituting into (9) for $\dot{V}_1$ using (6) and for $\dot{z}_2$ using (8), we obtain

$$\dot{V}_2 = -k_1 \|z_1\|^2 + z_2^\top (g_3 - \hat{a}uR_3 + \hat{d}_f - \dot{v}_d + (1 - k_1^2) z_1 + k_1 z_2 - \tilde{a}uR_3 + \tilde{d}_f).$$

Adding and subtracting $k_2 z_2^\top z_2$ in the above equation, where $k_2 > 0$ is the controller gain, we obtain

$$\begin{aligned} \dot{V}_2 = & -k_1 \|z_1\|^2 - k_2 \|z_2\|^2 + z_2^\top (g_3 - \hat{a}uR_3 + \hat{d}_f - \dot{v}_d + (1 - k_1^2) z_1 \\ & + (k_1 + k_2) z_2) + z_2^\top (\tilde{d}_f - u\tilde{a}R_3). \end{aligned} \tag{10}$$

We define the error state as

$$z_3 = g_3 - \hat{a}uR_3 + \hat{d}_f - \dot{v}_d + (1 - k_1^2) z_1 + (k_1 + k_2) z_2, \tag{11}$$

and note its dependence on the estimated parameters $\hat{a}$ and $\hat{d}_f$. Substituting (11) into (10) gives

$$\dot{V}_2 = -k_1 \|z_1\|^2 - k_2 \|z_2\|^2 + z_2^\top z_3 + z_2^\top (\tilde{d}_f - u\tilde{a}R_3). \tag{12}$$

Substituting (11) into (8) gives

$$\dot{z}_2 = z_3 - z_1 - k_2 z_2 - \tilde{a}uR_3 + \tilde{d}_f. \tag{13}$$

Proceeding to the next stage of the backstepping design, we compute the time derivative of (11) as

$$\dot{z}_3 = -\dot{\hat{a}}uR_3 - \hat{a}\dot{u}R_3 - \hat{a}u\dot{R}_3 + \dot{\hat{d}}_f - \ddot{v}_d + (1 - k_1^2)\dot{z}_1 + (k_1 + k_2)\dot{z}_2.$$

Substituting (7) and (13) into the last equation, we obtain

$$\begin{aligned} \dot{z}_3 = & -\dot{\hat{a}}uR_3 - \hat{a}\dot{u}R_3 - \hat{a}uR\mathrm{S}(\omega)e_3 + \dot{\hat{d}}_f - \ddot{v}_d + (1 - k_1^2)(-k_1 z_1 + z_2) \\ & + (k_1 + k_2)(z_3 - z_1 - k_2 z_2 - \tilde{a}uR_3 + \tilde{d}_f). \end{aligned}$$

Rearranging this expression gives

$$\begin{aligned} \dot{z}_3 = & -\dot{\hat{a}}uR_3 - \hat{a}\dot{u}R_3 - \hat{a}uR\mathrm{S}(\omega)e_3 + \dot{\hat{d}}_f - \ddot{v}_d + (k_1^3 - k_2 - 2k_1) z_1 \\ & + (1 - k_2(k_1 + k_2) - k_1^2) z_2 + (k_1 + k_2) z_3 - (k_1 + k_2)\tilde{a}uR_3 + (k_1 + k_2)\tilde{d}_f. \end{aligned} \tag{14}$$

For the above dynamics, consider the Lyapunov function $V_3 = V_2 + \frac{1}{2} z_3^\top z_3$. Taking the time derivative of V_3 and using (10), we obtain

$$\dot{V}_3 = -k_1 \|z_1\|^2 - k_2 \|z_2\|^2 + z_2^\top z_3 + z_2^\top (\tilde{d}_f - u\tilde{a}R_3) + z_3^\top \dot{z}_3.$$

Substituting (14) into the last equation leads to

$$\begin{aligned}\dot{V}_3 = &- k_1\|z_1\|^2 - k_2\|z_2\|^2 + z_3^\top\big(z_2 - \dot{\hat{a}}uR_3 - \hat{a}\dot{u}R_3 - \hat{a}uR\mathrm{S}(\omega)e_3 + \dot{\tilde{d}}_f - \ddot{v}_d \\ &+ (k_1^3 - k_2 - 2k_1)z_1 + (1 - k_2(k_1+k_2) - k_1^2)z_2 + (k_1+k_2)z_3 \\ &- (k_1+k_2)\tilde{a}uR_3 + (k_1+k_2)\tilde{d}_f\big) - \tilde{a}z_2^\top uR_3 + \tilde{d}_f^\top z_2.\end{aligned}$$

Adding and subtracting $k_3 z_3^\top z_3$ from the last expression, where $k_3 > 0$ is the controller gain, and simplifying gives

$$\begin{aligned}\dot{V}_3 = &- k_1\|z_1\|^2 - k_2\|z_2\|^2 - k_3\|z_3\|^2 + z_3^\top\big(-\dot{\hat{a}}uR_3 - \hat{a}\dot{u}R_3 - \hat{a}uR\mathrm{S}(\omega)e_3 + \dot{\tilde{d}}_f \\ &- \ddot{v}_d + (k_1^3 - k_2 - 2k_1)z_1 + (2 - k_2(k_1+k_2) - k_1^2)z_2 + (k_1+k_2+k_3)z_3\big) \\ &+ (\tilde{d}_f - \tilde{a}uR_3)^\top(z_2 + (k_1+k_2)z_3).\end{aligned}$$

In order to simplify this expression, we define

$$\sigma_1 = (k_1^3 - k_2 - 2k_1)z_1 + (2 - k_2(k_1+k_2) - k_1^2)z_2 + (k_1+k_2+k_3)z_3 - \ddot{v}_d, \tag{15a}$$

$$\sigma_2 = z_2 + (k_1+k_2)z_3. \tag{15b}$$

Now, consider a modified Lyapunov function:

$$V_{3b} = V_3 + \frac{1}{2\lambda}\tilde{a}^2 + \frac{1}{2k_{d_f}}\tilde{d}_f^\top\tilde{d}_f, \tag{16}$$

where $k_{d_f} > 0, \lambda > 0$ are controller gains. The time derivative of V_{3b} is

$$\begin{aligned}\dot{V}_{3b} = &- k_1\|z_1\|^2 - k_2\|z_2\|^2 - k_3\|z_3\|^2 + z_3^\top\big(-\dot{\hat{a}}uR_3 - \hat{a}\dot{u}R_3 - \hat{a}uR\mathrm{S}(\omega)e_3 + \dot{\tilde{d}}_f \\ &+ \sigma_1\big) + (\tilde{d}_f - \tilde{a}uR_3)^\top\sigma_2 + \frac{1}{\lambda}\tilde{a}\dot{\tilde{a}} + \frac{1}{k_{d_f}}\tilde{d}_f^\top\dot{\tilde{d}}_f.\end{aligned} \tag{17}$$

Since d_f is constant, we have $\dot{\tilde{d}}_f = -\dot{\hat{d}}_f$. Hence, (17) becomes

$$\begin{aligned}\dot{V}_{3b} = &- k_1\|z_1\|^2 - k_2\|z_2\|^2 - k_3\|z_3\|^2 + z_3^\top\big(-\dot{\hat{a}}uR_3 - \hat{a}\dot{u}R_3 \\ &- \hat{a}uR\mathrm{S}(\omega)e_3 + \dot{\hat{d}}_f + \sigma_1\big) + \tilde{a}\left(\frac{\dot{\tilde{a}}}{\lambda} - uR_3^\top\sigma_2\right) - \tilde{d}_f^\top\left(\frac{\dot{\hat{d}}_f}{k_{d_f}} - \sigma_2\right).\end{aligned}$$

Adding and subtracting $k_{d_f}z_3^\top\sigma_2$ yields

$$\begin{aligned}\dot{V}_{3b} = &- k_1\|z_1\|^2 - k_2\|z_2\|^2 - k_3\|z_3\|^2 + z_3^\top\big(-\dot{\hat{a}}uR_3 - \hat{a}\dot{u}R_3 - \hat{a}uR\mathrm{S}(\omega)e_3 \\ &+ \dot{\hat{d}}_f - k_{d_f}\sigma_2 + k_{d_f}\sigma_2 + \sigma_1\big) + \tilde{a}\left(\frac{\dot{\tilde{a}}}{\lambda} - uR_3^\top\sigma_2\right) - \tilde{d}_f^\top\left(\frac{\dot{\hat{d}}_f}{k_{d_f}} - \sigma_2\right),\end{aligned}$$

and simplification gives

$$\begin{aligned}\dot{V}_{3b} = &- k_1\|z_1\|^2 - k_2\|z_2\|^2 - k_3\|z_3\|^2 + z_3^\top(-\dot{\hat{a}}uR_3 - \hat{a}\dot{u}R_3 \\ &- \hat{a}uR\mathrm{S}(\omega)e_3 + \sigma_1 + k_{d_f}\sigma_2) + (\tilde{d}_f - k_{d_f}z_3)^\top\left(\sigma_2 - \frac{\dot{\hat{d}}_f}{k_{d_f}}\right) + \tilde{a}\left(\frac{\dot{\tilde{a}}}{\lambda} - uR_3^\top\sigma_2\right).\end{aligned} \tag{18}$$

Observe that

$$\begin{aligned}\sigma_1 + k_{d_f}\sigma_2 =& RR^\top(\sigma_1 + k_{d_f}\sigma_2) = RIR^\top(\sigma_1 + k_{d_f}\sigma_2)\\ =& R(I - e_3e_3^\top + e_3e_3^\top)R^\top(\sigma_1 + k_{d_f}\sigma_2)\\ =& \big(R(I - e_3e_3^\top)R^\top + R_3R_3^\top\big)(\sigma_1 + k_{d_f}\sigma_2).\end{aligned}$$

Hence,

$$\begin{aligned}\dot{V}_{3b} =& -k_1\|z_1\|^2 - k_2\|z_2\|^2 - k_3\|z_3\|^2 + z_3^\top\big[-\dot{\hat{a}}uR_3 - \hat{a}\dot{u}R_3\\ &+ R_3R_3^\top(\sigma_1 + k_{d_f}\sigma_2) - \hat{a}uR\mathrm{S}(\omega)e_3 + R(I - e_3e_3^\top)R^\top(\sigma_1 + k_{d_f}\sigma_2)\big]\\ &+ (\tilde{d}_f - k_{d_f}z_3)^\top\left(\sigma_2 - \frac{\dot{\hat{d}}_f}{k_{d_f}}\right) + \tilde{a}\left(\frac{\dot{\tilde{a}}}{\lambda} - uR_3^\top\sigma_2\right).\end{aligned}$$

Factoring out R_3 from the first three terms inside the square brackets and equating them to zero defines a control law for u. That is, we let

$$\hat{a}\dot{u} + \dot{\hat{a}}u = R_3^\top(\sigma_1 + k_{d_f}\sigma_2). \tag{19}$$

Therefore,

$$\begin{aligned}\dot{V}_{3b} =& -k_1\|z_1\|^2 - k_2\|z_2\|^2 - k_3\|z_3\|^2 + z_3^\top R\big(-\hat{a}u\mathrm{S}(\omega)e_3\\ &+ (I - e_3e_3^\top)R^\top(\sigma_1 + k_{d_f}\sigma_2)\big) + (\tilde{d}_f - k_{d_f}z_3)^\top\left(\sigma_2 - \frac{\dot{\hat{d}}_f}{k_{d_f}}\right) + \tilde{a}\left(\frac{\dot{\tilde{a}}}{\lambda} - uR_3^\top\sigma_2\right).\end{aligned} \tag{20}$$

We define $\omega_d \in \mathbb{R}^3$ as the desired angular velocity. The term $\hat{a}u\mathrm{S}(\omega)e_3$ in (20) can be interpreted as a virtual control, whose desired value is taken as

$$\hat{a}u\mathrm{S}(\omega_d)e_3 = (I - e_3e_3^\top)R^\top(\sigma_1 + k_{d_f}\sigma_2).$$

Since $\mathrm{S}(\omega_d)e_3 = -\mathrm{S}(e_3)\omega_d$, the last equation can be rewritten as

$$\hat{a}u\mathrm{S}(e_3)\omega_d = -(I - e_3e_3^\top)R^\top(\sigma_1 + k_{d_f}\sigma_2). \tag{21}$$

Extracting individual components of $\omega_d = [\omega_{d1}, \omega_{d2}, \omega_{d3}]^\top$, we have

$$\omega_{d1} = -\frac{e_2^\top}{\hat{a}u}(I - e_3e_3^\top)R^\top(\sigma_1 + k_{d_f}\sigma_2) = -R_2^\top(\sigma_1 + k_{d_f}\sigma_2)/(\hat{a}u), \tag{22}$$

$$\omega_{d2} = \frac{e_1^\top}{\hat{a}u}(I - e_3e_3^\top)R^\top(\sigma_1 + k_{d_f}\sigma_2) = R_1^\top(\sigma_1 + k_{d_f}\sigma_2)/(\hat{a}u), \tag{23}$$

where R_1 and $R_2 \in \mathbb{R}^3$ are the first and second columns of R. We can now rewrite (20) as

$$\begin{aligned}\dot{V}_{3b} =& -k_1\|z_1\|^2 - k_2\|z_2\|^2 - k_3\|z_3\|^2 + z_3^\top\hat{a}uR\mathrm{S}(e_3)(\omega - \omega_d)\\ &+ (\tilde{d}_f - k_{d_f}z_3)^\top\left(\sigma_2 - \frac{\dot{\hat{d}}_f}{k_{d_f}}\right) + \tilde{a}\left(\frac{\dot{\tilde{a}}}{\lambda} - uR_3^\top\sigma_2\right)\end{aligned} \tag{24}$$

Now, consider the following parameter update laws:

$$\begin{aligned}\dot{\hat{d}}_f =& k_{d_f}\sigma_2,\\ \dot{\hat{a}} =& -\lambda uR_3^\top\sigma_2,\end{aligned} \tag{25}$$

Substituting these adaptive laws into (24), we have

$$\dot{V}_{3b} = -k_1\|z_1\|^2 - k_2\|z_2\|^2 - k_3\|z_3\|^2 + z_3^\top \hat{a}u R\mathrm{S}(e_3)(\omega - \omega_d). \tag{26}$$

Let the error in angular velocity be $z_4 = \omega - \omega_d$. Using (3d), we can write

$$J\dot{z}_4 = J\dot{\omega} - J\dot{\omega}_d = -\mathrm{S}(\omega)J\omega + \tau + d_\tau - J\dot{\omega}_d. \tag{27}$$

Define

$$\begin{aligned}\bar{\omega}_d = &-\frac{1}{\hat{a}u}(\dot{\hat{a}}u + \hat{a}\dot{u})(I - e_3e_3^T)\omega_d + \frac{1}{\hat{a}u}\mathrm{S}^\top(e_3)\mathrm{S}(\omega)R^T(\sigma_1 + k_{d_f}\sigma_2)\\ &-\frac{1}{\hat{a}u}\mathrm{S}^\top(e_3)R^T(\bar{\sigma}_1 + k_{d_f}\bar{\sigma}_2) + \dot{\omega}_{d3}e_3,\end{aligned}$$

Using J_v instead of J, we have

$$J\bar{\omega}_d = \Psi(\bar{\omega}_d)J_v, \tag{28}$$

where

$$\Psi(\bar{\omega}_d) = \begin{bmatrix} \bar{\omega}_{d1} & 0 & 0 & \bar{\omega}_{d2} & 0 & \bar{\omega}_{d3} \\ 0 & \bar{\omega}_{d2} & 0 & \bar{\omega}_{d1} & \bar{\omega}_{d3} & 0 \\ 0 & 0 & \bar{\omega}_{d3} & 0 & \bar{\omega}_{d2} & \bar{\omega}_{d1} \end{bmatrix}.$$

Therefore, (27) can be rewritten as

$$J\dot{z}_4 = -(\Phi(\omega) + \Psi(\dot{\omega}_d))J_v + \tau + d_\tau. \tag{29}$$

Substituting $J_v = \hat{J}_v + \tilde{J}_v$ and $d_\tau = \hat{d}_\tau + \tilde{d}_\tau$ into (29) gives

$$J\dot{z}_4 = -(\Phi(\omega) + \Psi(\dot{\omega}_d))(\hat{J}_v + \tilde{J}_v) + \tau + \hat{d}_\tau + \tilde{d}_\tau. \tag{30}$$

Now, consider the Lyapunov function

$$V_4 = V_{3b} + \frac{1}{2}z_4^\top Jz_4 + \frac{1}{2k_{d_\tau}}\tilde{d}_\tau^\top\tilde{d}_\tau + \frac{1}{2}\tilde{J}_v^\top\Gamma^{-1}\tilde{J}_v, \tag{31}$$

where $k_{d_\tau} > 0$ and $\Gamma > 0 \in \mathbb{R}^{6\times6}$ are controller gains. Differentiating (31) with respect to time gives

$$\dot{V}_4 = \dot{V}_{3b} + z_4^\top J\dot{z}_4 + \frac{1}{k_{d_\tau}}\tilde{d}_\tau^\top\dot{\tilde{d}}_\tau + \tilde{J}_v^\top\Gamma^{-1}\dot{\tilde{J}}_v. \tag{32}$$

Substituting (26) and (30) into (32) gives

$$\begin{aligned}\dot{V}_4 = &-k_1\|z_1\|^2 - k_2\|z_2\|^2 - k_3\|z_3\|^2 + z_3^\top\hat{a}uR\mathrm{S}(e_3)z_4\\ &+ z_4^\top(-(\Phi(\omega) + \Psi(\dot{\omega}_d))(\hat{J}_v + \tilde{J}_v) + \tau + \hat{d}_\tau + \tilde{d}_\tau) + \frac{1}{k_{d_\tau}}\tilde{d}_\tau^\top\dot{\tilde{d}}_\tau + \tilde{J}_v^\top\Gamma^{-1}\dot{\tilde{J}}_v.\end{aligned} \tag{33}$$

Let $k_4 > 0$ be the controller gain. By adding and subtracting $k_4z_4^\top z_4$ in the above expression and factoring $z_4^\top$, we obtain

$$\begin{aligned}\dot{V}_4 = &-k_1\|z_1\|^2 - k_2\|z_2\|^2 - k_3\|z_3\|^2 - k_4\|z_4\|^2\\ &+ z_4^\top(\hat{a}u\mathrm{S}^\top(e_3)R^\top z_3 + k_4z_4 - (\Phi(\omega) + \Psi(\dot{\omega}_d))\hat{J}_v + \tau + \hat{d}_\tau)\\ &+ \tilde{J}_v^\top(\Gamma^{-1}\dot{\tilde{J}}_v - (\Phi(\omega) + \Psi(\dot{\omega}_d))^\top z_4) + \tilde{d}_\tau^\top(\frac{1}{k_{d_\tau}}\dot{\tilde{d}}_\tau + z_4).\end{aligned} \tag{34}$$

At this point, we assign the expression for input τ:

$$\tau = \hat{a}u\mathrm{S}(e_3)R^\top z_3 - k_4z_4 + (\Phi(\omega) + \Psi(\dot{\omega}_d))\hat{J}_v - \hat{d}_\tau, \tag{35}$$

and define the parameter update laws

$$\begin{aligned}\dot{\hat{J}}_v &= -\Gamma(\Phi(\omega) + \Psi(\dot{\omega}_d))^\top z_4, \\ \dot{\hat{d}}_\tau &= k_{d_\tau} z_4.\end{aligned} \tag{36}$$

Using $\dot{\hat{d}}_\tau = -\dot{\hat{d}}_\tau$ and $\dot{\hat{J}}_v = -\dot{\hat{J}}_v$ since J_v and d_τ are constants and substituting (35) and (36) into (34), we obtain

$$\dot{V}_4 = -k_1\|z_1\|^2 - k_2\|z_2\|^2 - k_3\|z_3\|^2 - k_4\|z_4\|^2, \tag{37}$$

which is negative semi-definite.

Theorem 1. *Consider the UAM dynamics* (3) *and assume that* $\dot{a} = 0$, $\dot{d}_f = 0$, $\dot{d}_\tau = 0$, $\dot{J}_v = 0$, *and* $u > 0$, $\hat{a} > 0$. *Given a smooth time-varying trajectory* $p_d(t)$, *feedback law* (35) *with* $k_1, k_2, k_3, k_4 > 0$, *and parameter update laws* (25) *and* (36) *with* $k_{d_f}, k_{d_\tau}, \lambda$, *and* $\Gamma > 0$, *then the tracking error* $z^\top = [z_1^\top, z_2^\top, z_3^\top,$ *and* $z_4^\top]$ *is globally asymptotically convergent to* 0 *and the parameter estimates* $\hat{a}, \hat{d}_f, \hat{d}_\tau$ *and* $\hat{J}_v$ *are bounded.*

Proof. Consider the quadratic positive definite Lyapunov function V_4 in (31). According to [36] (Lemma 4.3), there exist two positive definite functions that form the lower and upper bounds of V_4. The time derivative of V_4 after substitution of (25), (35), and (36) is a negative semi-definite function. Using Barbalat's lemma [36] (Theorem 8.4), we can conclude that $z \to 0$ as $t \to \infty$, and the parameter and disturbance estimates $\hat{a}$, $\hat{d}_f$, $\hat{d}_\tau$, and $\hat{J}_v$ are bounded. Since V_4 is radially unbounded, we conclude that the equilibrium point $z = 0$ is globally asymptotically stable. □

3.2. Position and Yaw Tracking Control

Thus far, the adaptive backstepping control design has achieved trajectory tracking for p. Since the UAV has four control inputs, we can extend the control to track UAV heading, which is practically relevant for manipulation tasks. We identify UAV heading with yaw angle $\psi \in (-\pi, \pi]$. Let the desired UAV yaw trajectory be $\psi_d \in (-\pi, \pi]$ and define the tracking error as $z_\psi = \psi - \psi_d$. Let

$$V_\psi = \frac{1}{2} z_\psi^2. \tag{38}$$

Thus,

$$\dot{V}_\psi = z_\psi \dot{z}_\psi = z_\psi(\dot{\psi} - \dot{\psi}_d). \tag{39}$$

The rotational kinematics (1) can be expressed in terms of ZYX or 321 Euler angles by substituting the expression for R as a function of Euler angles into that equation. We obtain

$$\omega = W(\theta, \phi)\dot{\eta} \tag{40}$$

where $\eta = [\phi, \theta, \psi]^\top$, ϕ denotes roll, and θ denotes pitch, and

$$W(\theta, \phi) = \begin{bmatrix} 1 & 0 & -\mathrm{s}_\theta \\ 0 & \mathrm{c}_\phi & \mathrm{s}_\phi \mathrm{c}_\theta \\ 0 & -\mathrm{s}_\phi & \mathrm{c}_\phi \mathrm{c}_\theta \end{bmatrix}$$

where $\mathrm{c}_\theta = \cos\theta$ and $\mathrm{s}_\theta = \sin\theta$. Since $|W| = \mathrm{c}_\theta$, W is invertible for $\theta \neq \pm\pi/2$, and the rotational kinematics (41) can be written as

$$\dot{\eta} = W(\theta, \phi)^{-1}\omega \tag{41}$$

Hence, taking the third component of (40), the yaw rate can be expressed in terms of the angular velocity as $\dot{\psi} = e_3^\top W^{-1}(\theta, \phi)\omega$. The inverse of W is

$$W^{-1}(\theta, \phi) = \begin{bmatrix} 1 & \mathrm{t}_\theta \mathrm{s}_\phi & \mathrm{t}_\theta \mathrm{c}_\phi \\ 0 & \mathrm{c}_\phi & -\mathrm{s}_\phi \\ 0 & \frac{\mathrm{s}_\phi}{\mathrm{c}_\theta} & \frac{\mathrm{c}_\phi}{\mathrm{c}_\theta} \end{bmatrix}$$

where $\mathrm{t}_\theta = \tan\theta$ Therefore, we can write (39) as

$$\dot{V}_\psi = z_\psi \dot{z}_\psi = z_\psi (e_3^\top W^{-1}\omega - \dot{\psi}_d)$$

Adding and subtracting $k_\psi z_\psi^2$, where $k_\psi > 0$ is the control gain, gives

$$\dot{V}_\psi = -k_\psi z_\psi^2 + z_\psi (k_\psi z_\psi + e_3^\top W^{-1}\omega - \dot{\psi}_d) \tag{42}$$

In order to define the third component of the desired angular velocity ω_d, we use

$$e_3^\top W^{-1}\omega_d = \frac{\mathrm{s}_\phi}{\mathrm{c}_\theta}\omega_{d2} + \frac{\mathrm{c}_\phi}{\mathrm{c}_\theta}\omega_{d3} = -k_\psi z_\psi + \dot{\psi}_d \tag{43}$$

Solving this equation for ω_{d3} gives

$$\omega_{d3} = \frac{\mathrm{c}_\theta}{\mathrm{c}_\phi}(-k_\psi z_\psi + \dot{\psi}_d + \frac{\mathrm{s}_\phi}{\mathrm{c}_\theta}\omega_{d2}) = \frac{\mathrm{c}_\theta}{\mathrm{c}_\phi}(-k_\psi z_\psi + \dot{\psi}_d) + \mathrm{t}_\phi \omega_{d2}, \tag{44}$$

where ω_{d2} is given in (23). Substituting (43) into (42) results in

$$\begin{aligned} \dot{V}_\psi &= -k_\psi z_\psi^2 + z_\psi (e_3^\top W^{-1}(\omega - \omega_d)) \\ &= -k_\psi z_\psi^2 + z_\psi (e_3^\top W^{-1} z_4) \\ &= -k_\psi z_\psi^2 + z_4^\top z_\psi {W^{-1}}^\top e_3. \end{aligned} \tag{45}$$

We are now ready to state the stability result for the position–yaw tracking controller.

Theorem 2. *Consider the UAM dynamics (3) and assume that $\dot{a} = 0$, $\dot{d}_f = 0$, $\dot{d}_\tau = 0$, $\dot{J}_v = 0$, $u > 0$, and $\hat{a} > 0$. Given a smooth trajectory $p_d(t)$, $\psi_d(t)$, control (19) and*

$$\tau = -z_\psi W^{-T} e_3 - \hat{a} u S(e_3) R^\top z_3 - k_4 z_4 + (\Phi(\omega) + \Psi(\dot{\omega}_d))\hat{J}_v - \hat{d}_\tau \tag{46}$$

with $k_1, k_2, k_3, k_4 > 0$ and parameter update laws (25) and (36) with k_{d_f}, k_{d_τ}, and $\lambda, \Gamma > 0$, then the tracking error $z^\top = [z_1^\top, z_2^\top, z_3^\top, z_4^\top, z_\psi]$ converges asymptotically to 0 while the estimates $\hat{a}, \hat{d}_f, \hat{d}_\tau$ and $\hat{J}_v$ are bounded.

Proof. Consider the Lyapnouv function $V_{4,\psi} = V_4 + V_\psi$ with time derivative

$$\dot{V}_{4,\psi} = \dot{V}_4 + \dot{V}_\psi. \tag{47}$$

Substituting for $\dot{V}_4$ using (34) and using parameter update laws (36) and the expression for $\dot{V}_\psi$ in (45) gives

$$\begin{aligned} \dot{V}_{4,\psi} = &- k_1\|z_1\|^2 - k_2\|z_2\|^2 - k_3\|z_3\|^2 - k_4\|z_4\|^2 - k_\psi z_\psi^2 + z_4^\top z_\psi {W^{-1}}^\top e_3 \\ &+ z_4^\top (-\hat{a} u \mathrm{S}^\top(e_3) R^\top z_3 + k_4 z_4 - (\Phi(\omega) + \Psi(\dot{\omega}_d))\hat{J}_v + \tau + \hat{d}_\tau) \end{aligned} \tag{48}$$

Substituting (46) gives

$$\dot{V}_{4,\psi} = -k_1\|z_1\|^2 - k_2\|z_2\|^2 - k_3\|z_3\|^2 - k_4\|z_4\|^2 - k_\psi\|z_\psi\|^2 \tag{49}$$

which is negative semi-definite. As in the proof of Theorem 1, we conclude that $z \to 0$ as $t \to \infty$ and the parameters remain bounded. □

Remark 1. *The controllers presented in* (35) *and* (46) *depend on* $\dot{\omega}_d$*; however, the above derivation gives an expression for* ω_d*. The value of* $\dot{\omega}_d$ *can be obtained numerically from the low-pass-filtered finite difference. The algebraic expression for* ω_d *depends on* $\tilde{d}_f$*, which is not known. In addition, the unknown inertia vector* J_v *in the angular velocity dynamics complicates the stability proof. Work in [33] provides further details for alternate solutions to this problem.*

Other underactuated UAMs, which are based on traditional helicopters [37,38] or hexacopters [8], could be controlled using the proposed scheme with no modification other than to the mixing subsystem that maps the four-dimensional force/torque to the physical inputs. For example, this mixing is built into the PX4 autopilot [39]. Furthermore, the type of manipulator arm is not important as its dynamics are treated as a disturbance or parameter uncertainty. Hence, the approach could be applied to UAMs such as [8], where a hexarotor carries a four-DoF arm, or [9], which considers a quadrotor with a three-DoF arm.

4. Simulation Results

This section presents numerical simulations using MATLAB R2024b and the Simscape Multibody toolbox to validate our control design. The files used to generate these simulations can be found at https://github.com/ANCL/UAM_control (accessed on 1 June 2025). A multibody simulation is necessary to avoid the complexity of simulating the closed loop in a traditional state-space format. The UAM used in the simulation is shown in Figure 3. The arm is a three-link, two-DoF manipulator with two revolute joints. Link 1 is attached to the CoM of the UAV and rotates in the $b_1 - b_3$ plane about the origin of $\mathcal{B}$. Link 2 is a revolute joint, which also rotates in the same plane. Link 3 is fixed to Link 2 and acts as a payload mass. The UAV and arm parameters are given in Tables 1 and 2 respectively. We consider three simulations: a figure-of-eight desired position with fixed and moving arm cases and a pick-and-place operation.

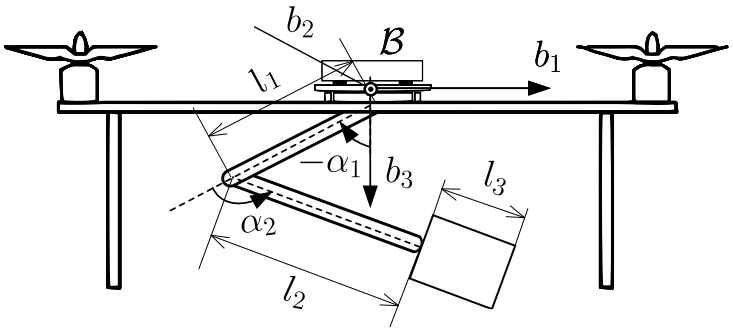


Figure 3. UAM configuration.

Table 1. UAV parameters.

Parameter	Value	Parameter	Value
m	1.6 kg	J_{xx}, J_{yy}	0.03 kg m^2
J_{zz}	0.05 kg m^2	J_{xy}, J_{zx}, J_{yz}	0.0 kg m^2

Table 2. Arm parameters.

Parameter	Link 1	Link 2	Link 3
Joint Type	Revolute	Revolute	Fixed
Mass (kg)	0.1	0.1	0.1
Length (m)	0.2	0.3	0.1
Inertia (kg m^2)	$[7.508, 7.533, 0.0417] \times 10^{-4}$	$[7.508, 7.533, 0.0417] \times 10^{-4}$	$[1.667, 1.667, 1.667] \times 10^{-4}$

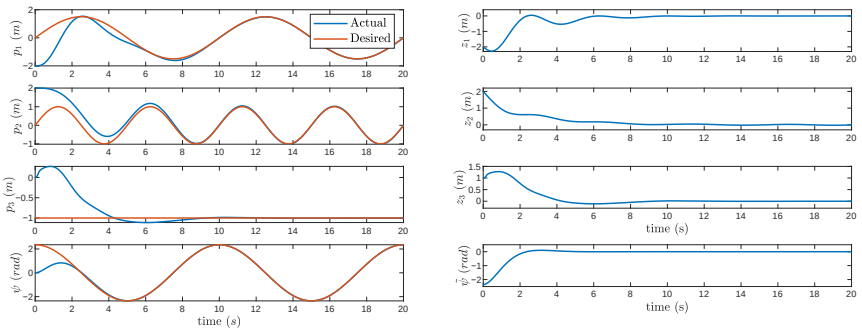
4.1. Figure-of-Eight Reference Trajectory

For the figure-of-eight trajectory, in addition to the coupling forces and torques due to the arm, we consider a constant external disturbance force of $[0.2, 0.2, 0.2]^\top$ N acting at the UAV CoM. The controller gains used for all simulations are given in Table 3. The initial conditions are $p(0) = [-2, 2, 0]^\top$ m, $v(0) = 0$ m s^{-1}, $\eta(0) = 0$ rad and $\omega(0) = 0$ rad s^{-1}, $\hat{a}(0) = \frac{1}{0.7m}$, and $\hat{J}_v(0) = 0.6J_v$, i.e., we consider a 30% error in mass and a 40% error in inertia initially. The initial conditions for the disturbances are $\hat{d}_f(0) = \hat{d}_\tau(0) = 0$.

Table 3. Control gains.

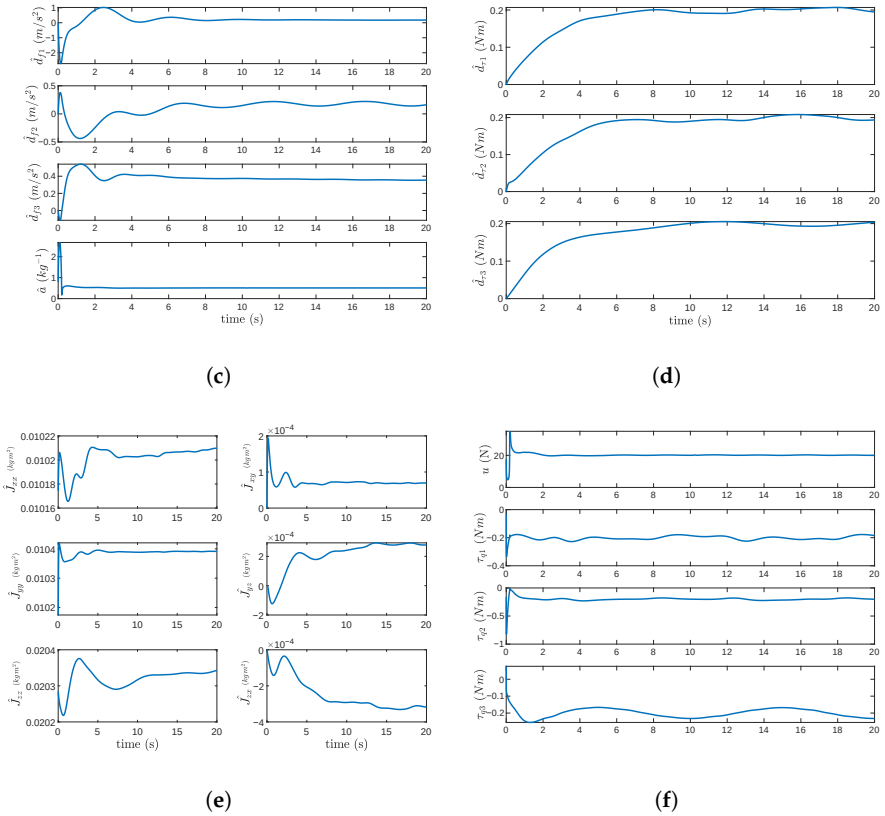
Parameter	Value	Parameter	Value
k_1	0.4	k_2	0.5
k_3	0.5	k_4	7
k_{d_f}	1	λ	3
Γ	0.001	k_{d_τ}	5
k_ψ	1		

Figure 4a–f present the simulation results for the fixed-arm case $\alpha_1 = \alpha_2 = 0$, where the arm is locked in the b_3 direction. The position tracking errors in Figure 4b converge to a small neighborhood of 0. The estimates $\hat{a}$, $\hat{d}_f$, $\hat{d}_\tau$, and $\hat{J}_v$ remain bounded. These estimates are shown in Figure 4c–e. We observe that in steady state these parameters are time-varying due to the time-varying reference trajectory. That is, the UAV must vary its attitude to track the position trajectory, and this creates a time-varying disturbance. Figure 4f shows the control inputs. The simulation results for the moving-arm case are shown in Figure 5a–f. The arm motion is given by $\alpha_1(t) = \frac{\pi}{3}\sin(\pi t)$ and $\alpha_2(t) = \frac{3\pi}{2}t$. Figure 5b presents the UAV CoM position errors, which remain small with only mild oscillations around the origin. Compared with the fixed-arm case, the steady-state error is somewhat larger but still acceptable from a practical standpoint. The estimated parameters and disturbances remain bounded and time-varying in steady state, with significant variation, as shown in Figure 5c–e. Figure 5f shows the control inputs.



(**a**) (**b**)

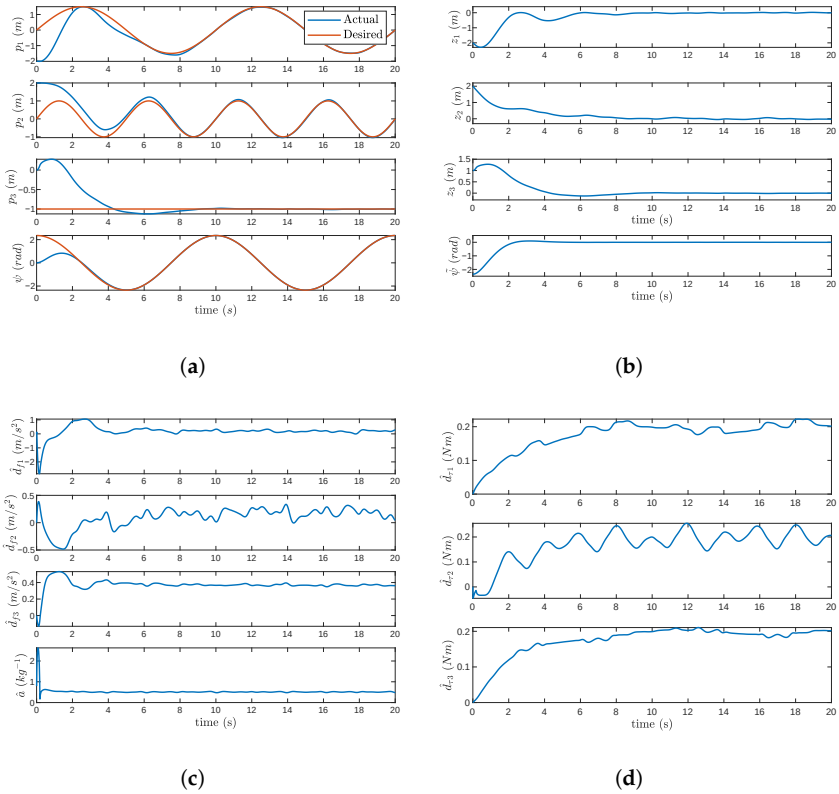
Figure 4. *Cont.*



(**c**) (**d**)

(**e**) (**f**)

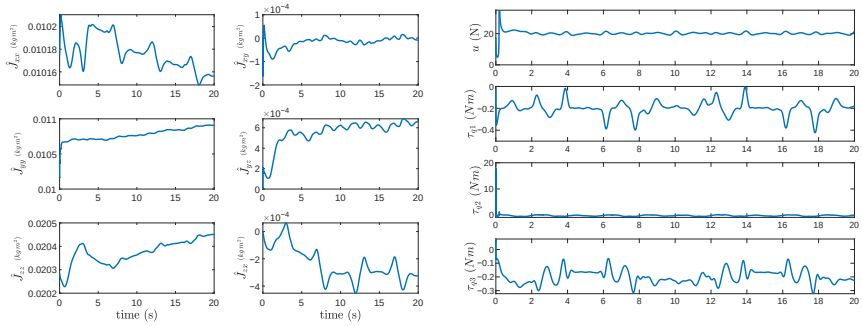
Figure 4. Results for fixed-arm configuration ($\alpha_1 = \alpha_2 = 0$). (**a**) Trajectories for p and ψ. (**b**) Tracking error. (**c**) Parameter estimates $\hat{d}_f$ and $\hat{a}$. (**d**) Parameter estimates $\hat{d}_\tau$. (**e**) Parameter estimates $\hat{J}$. (**f**) Inputs u and τ.



(**a**) (**b**)

(**c**) (**d**)

Figure 5. *Cont.*



(**e**) (**f**)

Figure 5. Results for the moving arm configuration. (**a**) Trajectories for p and ψ. (**b**) Tracking error. (**c**) Parameter estimates $\hat{d}_f$ and $\hat{a}$. (**d**) Parameter estimates $\hat{d}_\tau$. (**e**) Parameter estimates $\hat{J}$. (**f**) Inputs u and τ

4.2. Adaptation Comparison with Fixed-Parameter Case

This section assesses the performance of the proposed method compared to a method in the existing literature. In order to make a sensible and fair comparison, we choose to compare it with the design in [30]. This method shares certain elements with the proposed design. Both approaches use a backstepping methodology, but [30] does not adapt to inertial parameters a and J. In the adaptive case, all update laws (25) and (36) are active. In the fixed-parameter case, the updates for $\hat{a}$ and $\hat{J}_v$ are disabled, i.e., $\dot{\hat{a}} = 0$ and $\dot{\hat{J}}_v = 0$, so these estimates remain at their initial values. The disturbance-related estimates $\hat{d}_f$ and $\hat{d}_\tau$ continue to adapt, ensuring disturbance rejection. Both controllers use identical gains that are shown in Table 3.

Performance is evaluated using the settling time t_s and the steady-state nRMSE of the combined error norm e. For periodic responses, t_s is defined as the time taken to reach 5% of the steady state. The tracking error is normalized using the desired trajectory with

$$\varepsilon = \begin{bmatrix} \dfrac{p_1 - p_{d1}}{\max(p_{d1}) - \min(p_{d1})} \\ \dfrac{p_2 - p_{d2}}{\max(p_{d2}) - \min(p_{d2})} \\ \dfrac{p_3 - p_{d3}}{\max(p_{d3}) - \min(p_{d3})} \\ \dfrac{\psi - \psi_d}{\max(\psi_d) - \min(\psi_d)} \end{bmatrix} \in \mathbb{R}^4, \tag{50}$$

and we compute its norm

$$e = \|\varepsilon\|_2. \tag{51}$$

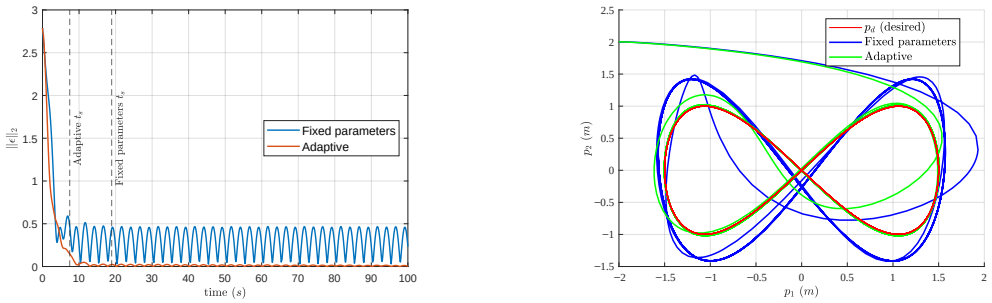
The steady-state nRMSE is computed over the interval $[t_s, T]$ as

$$\text{nRMSE} = \sqrt{\frac{1}{T - t_s} \int_{t_s}^{T} e^2 \, dt}. \tag{52}$$

The proposed method reduces t_s from 18.93 s to 7.45 s (approximately 61 % faster) and nRMSE from 33.3 % to 1.4 % (approximately 96 % reduction) in the fixed-arm case (Table 4, Figure 6a). In the moving-arm configuration, the improvements are similar: t_s drops from 12.60 s to 7.04 s and nRMSE from 33.6 % to 2.0 % (Table 5, Figure 7a). These results demonstrate that adaptation consistently accelerates convergence and tightens tracking accuracy under the added complexity of arm dynamics.

Table 4. Settling time t_s (s) and steady-state nRMSE (%) for the fixed-arm case.

Case	t_s (s)	SS nRMSE (%)
Fixed parameters	18.93	33.34
Adaptive	7.45	1.37

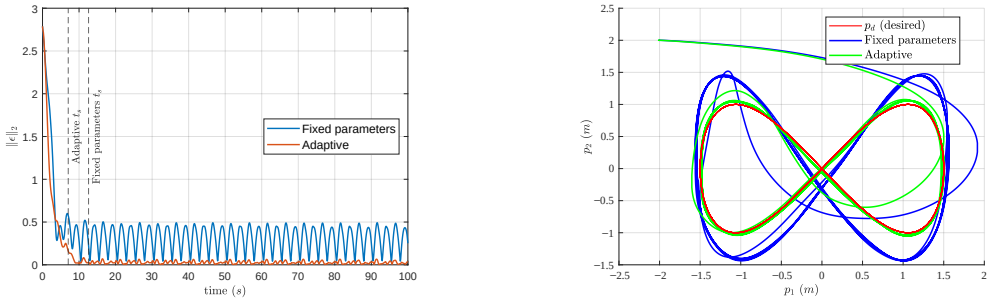


(**a**) Normalized error comparison (**b**) 2D top view

Figure 6. Fixed-arm configuration ($\alpha_1 = \alpha_2 = 0$): (**a**) normalized tracking error norm e for fixed-parameter vs. adaptive case; (**b**) 2D top-view trajectories with desired path.

Table 5. Settling time t_s (s) and steady-state nRMSE (%) for the moving-arm case.

Case	t_s (s)	SS nRMSE (%)
Fixed parameters	12.60	33.57
Adaptive	7.04	1.96



(**a**) Normalized error comparison (**b**) 2D top view

Figure 7. Moving-arm case: (**a**) normalized tracking error norm e for fixed-parameter vs. adaptive case; (**b**) 2D top-view trajectories with desired path.

4.3. Robustness to Parameter Variation

To evaluate robustness, ten simulations were performed with random UAM parameters and disturbances. The parameter range considered was ±30% for masses, ±40% for principal inertias, and ±15% for link lengths. Disturbances were randomized within ±250% of their nominal value. The adaptive controller was applied with the same fixed gains (Table 3) for all runs. Table 6 summarizes the results. All simulations converged within 6–8 s, with steady-state normalized RMSEs consistently around 1–3%. The variation across simulations was small: the standard deviation of t_s was less than 1 s and the standard deviation of steady-state nRMSE remained below 0.3%. These results indicate that, even under parameter uncertainty and different disturbance levels, the adaptive controller achieves robust tracking performance.

Table 6. Performance per case: settling time (5% criterion) and steady-state nRMSE (%) for fixed- and moving-arm configurations.

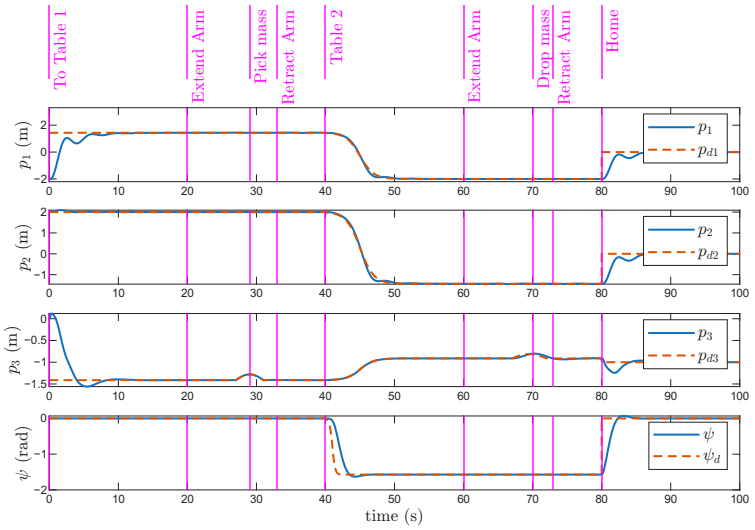
Case	Fixed Arm		Moving Arm	
	t_s (s)	SS nRMSE (%)	t_s (s)	SS nRMSE (%)
1	7.39	1.73	6.77	2.64
2	7.25	1.80	6.80	2.42
3	7.93	1.26	7.81	1.56
4	7.55	2.20	7.28	2.38
5	7.63	1.52	7.33	2.07
6	7.39	1.51	6.89	1.92
7	7.33	1.47	6.84	2.04
8	7.64	1.57	7.43	2.18
9	7.54	1.64	7.44	2.12
10	7.16	1.54	6.83	2.05
STD	0.25	0.26	0.29	0.29

4.4. Pick-and-Place

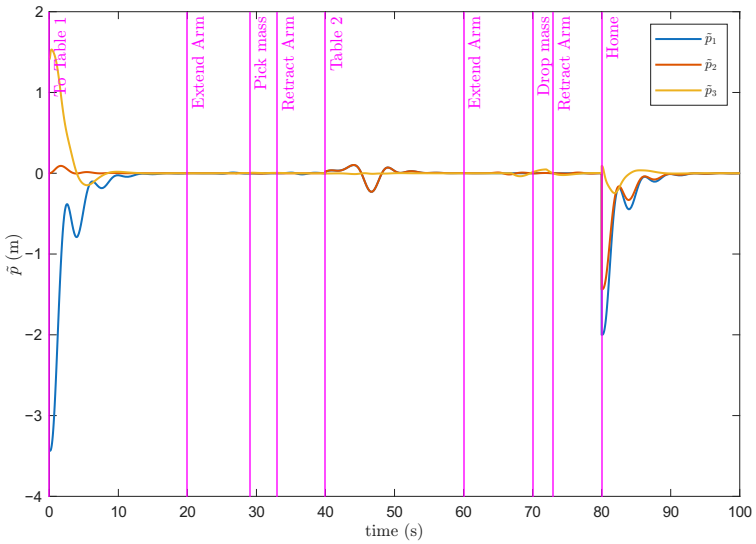
We now present a practical pick-and-place motion, where the UAM takes off to a target position, extends its arm, picks up a payload, flies it to a desired location, and places the payload at the desired location. Multiple "table" landmarks are created in MATLAB Simscape Multibody that correspond to the various locations of the task. A small cubic payload of mass 0.1kg and dimension 0.1m is attached to the end-effector. The UAV CoM start location is $p(0) = [-2, 2, 0]^\top$m. The first and second desired UAV CoM positions and yaws are denoted as Location 1 and Location 2, respectively. Location 1 is $p_d^1 = [1.4379, 2.0000, -1.4121]^\top$m, $\psi_d^1 = 0$ rad, and Location 2 is $p_d^2 = [-2, -1.4379, -0.9121]^\top$m, $\psi_d^2 = -\pi/2$ rad. When picking up the payload, the UAV position is lowered using a function $h(t_0) = [0, 0, 0.1\sin(\pi(t_0)/5))]^\top$. Table 7 shows the desired trajectory for the UAV and arm. The Home configuration for the arm is selected to be $\alpha_1 = -\pi/4, \alpha_2 = 3\pi/4$. The desired values of p and ψ are shown in Figure 8a. The position errors are given in Figure 8b. The figures label each phase of the task. Evidently, the figures show that tracking error is asymptotically convergent, as expected by the theory. In this task, the assumptions of Theorem 2 hold as the desired position, and the arm configuration is eventually constant. Hence, this simulation case illustrates a practical case where assumptions hold.

Table 7. Object pick-and-place sequence.

Time t	Desired Position p_d	Desired Yaw ψ_d	Arm Configuration	Cube Location
0	p_d^1	ψ_d^1	Home	Table 1
20	p_d^1	ψ_d^1	Extending	Table 1
27	$p_d^1 + h(t-27)$	ψ_d^1	Extended	Table 1
29	$p_d^1 + h(t-27)$	ψ_d^1	Extended	UAM
32	p_d^1	ψ_d^1	Retracting	UAM
40	$p_d^1 + \frac{p_d^2 - p_d^1}{1+\exp(-(t-45))}$	$\frac{\psi_d^2}{1+\exp(-(t-45))}$	Home	UAM
60	p_d^2	ψ_d^2	Extending	UAM
67	$p_d^2 + h(t-67)$	ψ_d^2	Extending	UAM
70	$p_d^2 + h(t-67)$	ψ_d^2	Extended	Table 2
73	p_d^2	ψ_d^2	Retracting	Table 2
80	$[0, 0, 0]^T$	0	Home	Table 2



(**a**)



(**b**)

Figure 8. Pick-and-place application results: (**a**) UAV pose and (**b**) position errors.

5. Conclusions

In this paper, we have presented a control design for a UAM consisting of a UAV and a multi-DoF robotic arm. The design is based on a UAV model that accounts for the arm's effect by including torque and force disturbances and parametric uncertainty. An adaptive backstepping control law is presented that achieves UAV CoM position and yaw tracking when disturbances and parameters are constant. Numerical simulations demonstrate that bounded tracking error results when disturbances and parameters are varying. A practical pick-and-place task illustrates a case where tracking error converges. Future work will involve indoor and outdoor experimental validation of the control with an open-source platform, as in [40]. An intermediate step for this validation is software-in-the-loop testing that includes various non-idealities such as actuator saturation, sampling effects, state estimation errors, and rotor drag [41].

Author Contributions: Methodology, M.A.R. and A.F.L.; Software, M.A.R. and M.E.E.; Validation, M.E.E.; Formal analysis, M.A.R. and A.F.L.; Writing—review & editing, A.F.L. and M.E.E.; Visualization, M.E.E. All authors have read and agreed to the published version of the manuscript.

Funding: This research was funded by the Natural Sciences and Engineering Council of Canada (NSERC) Grant RGPIN-2023-04156 and The Government of Alberta Major Innovation Fund Grant No. MIF-23-009.

Data Availability Statement: The data presented in this study are openly available at [https://github.com/ANCL/UAM_control], accessed on 1 June 2025.

Conflicts of Interest: The authors declare no conflicts of interest.

References

1. Villa, D.K.D.; Brandão, A.S.; Sarcinelli-Filho, M. A Survey on Load Transportation Using Multirotor UAVs. *J. Intell. Robot. Syst.* **2020**, *98*, 267–296. [CrossRef]
2. Watson, R.J.; Pierce, S.G.; Kamel, M.; Zhang, D.; MacLeod, C.N.; Dobie, G.; Bolton, G.; Dawood, T.; Nieto, J. Deployment of Contact-Based Ultrasonic Thickness Measurements Using Over-Actuated UAVs. In *European Workshop on Structural Health Monitoring, Proceedings of the European Workshop on Structural Health Monitoring (EWSHM 2020), Palermo, Italy, 6–9 July 2020*; Lecture Notes in Civil Engineering; Rizzo, P., Milazzo, A., Eds.; Springer: Cham, Switzerland, 2021; Volume 127, pp. 683–694. [CrossRef]
3. Bonyan Khamseh, H.; Janabi-Sharifi, F.; Abdessameud, A. Aerial manipulation—A literature survey. *Robot. Auton. Syst.* **2018**, *107*, 221–235. [CrossRef]
4. Ollero, A.; Tognon, M.; Suarez, A.; Lee, D.; Franchi, A. Past, Present, and Future of Aerial Robotic Manipulators. *IEEE Trans. Robot.* **2022**, *38*, 626–645. [CrossRef]
5. Albers, A.; Trautmann, S.; Howard, T.; Nguyen, T.A.; Frietsch, M.; Sauter, C. Semi-autonomous flying robot for physical interaction with environment. In Proceedings of the IEEE Conference on Robotics, Automation and Mechatronics, Singapore, 28–30 June 2010; pp. 441–446. [CrossRef]
6. Nguyen, H.; Lee, D. Hybrid force/motion control and internal dynamics of quadrotors for tool operation. In Proceedings of the IEEE/RSJ International Conference on Intelligent Robots and Systems (IROS), Tokyo, Japan, 3–7 November 2013; pp. 3458–3464. [CrossRef]
7. Mersha, A.Y.; Stramigioli, S.; Carloni, R. Variable impedance control for aerial interaction. In Proceedings of the IEEE/RSJ International Conference on Intelligent Robots and Systems (IROS), Chicago, IL, USA, 14–18 September 2014; pp. 3435–3440. [CrossRef]
8. Kim, S.; Choi, S.; Kim, H.; Shin, J.; Shim, H.; Kim, H.J. Robust Control of an Equipment-Added Multirotor Using Disturbance Observer. *IEEE Trans. Autom. Control* **2018**, *26*, 1524–1531. [CrossRef]
9. Jimenez-Cano, A.E.; Martin, J.; Heredia, G.; Ollero, A.; Cano, R. Control of an aerial robot with multi-link arm for assembly tasks. In Proceedings of the IEEE International Conference on Robotics and Automation (ICRA), Karlsruhe, Germany, 6–10 May 2013; pp. 4916–4921. [CrossRef]
10. Korpela, C.; Orsag, M.; Pekala, M.; Oh, P. Dynamic stability of a mobile manipulating unmanned aerial vehicle. In Proceedings of the IEEE International Conference on Robotics and Automation (ICRA), Karlsruhe, Germany, 6–10 May 2013; pp. 4922–4927. [CrossRef]
11. Kannan, S.; Olivares-Mendez, M.A.; Voos, H. Modeling and Control of Aerial Manipulation Vehicle with Visual sensor. *IFAC Proc. Vol.* **2013**, *46*, 303–309. [CrossRef]
12. Kannan, S.; Alma, M.; Olivares-Mendez, M.A.; Voos, H. Adaptive control of Aerial Manipulation Vehicle. In Proceedings of the IEEE International Conference on Control System, Computing and Engineering (ICCSCE), Penang, Malaysia, 28–30 November 2014; pp. 273–278. [CrossRef]
13. Khalifa, A.; Fanni, M.; Ramadan, A.; Abo-Ismail, A. Modeling and control of a new quadrotor manipulation system. In Proceedings of the First International Conference on Innovative Engineering Systems, Alexandria, Egypt, 7–9 December 2012; pp. 109–114. [CrossRef]
14. Samadikhoshkho, Z.; Lipsett, M. Decoupled Control Design of Aerial Manipulation Systems for Vegetation Sampling Application. *Drones* **2023**, *7*, 110. [CrossRef]
15. Ding, L.; Zhu, G.; Li, Y.; Wang, Y. Cable-Driven Unmanned Aerial Manipulator Systems for Water Sampling: Design, Modeling, and Control. *Drones* **2023**, *7*, 450. [CrossRef]

16. Lippiello, V.; Ruggiero, F. Exploiting redundancy in Cartesian impedance control of UAVs equipped with a robotic arm. In Proceedings of the IEEE/RSJ International Conference on Intelligent Robots and Systems (IROS), Vilamoura-Algarve, Portugal, 7–12 October 2012; pp. 3768–3773. [CrossRef]
17. Lippiello, V.; Ruggiero, F. Cartesian Impedance Control of a UAV with a Robotic Arm. In Proceedings of the 10th International IFAC Symposium on Robot Control, Dubrovnik, Croatia, 5–7 September 2012; pp. 704–709.
18. Kim, S.; Choi, S.; Kim, H.J. Aerial manipulation using a quadrotor with a two DOF robotic arm. In Proceedings of the IEEE/RSJ International Conference on Intelligent Robots and Systems (IROS), Tokyo, Japan, 3–7 November 2013; pp. 4990–4995. [CrossRef]
19. Yang, H.; Lee, D. Dynamics and control of quadrotor with robotic manipulator. In Proceedings of the IEEE International Conference on Robotics and Automation (ICRA), Hong Kong, China, 31 May–7 June 2014; pp. 5544–5549. [CrossRef]
20. Korpela, C.; Orsag, M.; Oh, P. Towards valve turning using a dual-arm aerial manipulator. In Proceedings of the IEEE/RSJ International Conference on Intelligent Robots and Systems (IROS), Chicago, IL, USA, 14–18 September 2014; pp. 3411–3416. [CrossRef]
21. Samadikhoshkho, Z.; Ghorbani, S.; Janabi-Sharifi, F.; Zareinia, K. Nonlinear control of aerial manipulation systems. *Aerosp. Sci. Technol.* **2020**, *104*, 105945. [CrossRef]
22. Li, H.; Li, Z.; Wu, T.; Dong, C.; Xu, Q.; Yang, Y.; Yu, X. A Novel Active Anti-Disturbance Control Strategy for Unmanned Aerial Manipulator Based on Variable Coupling Disturbance Compensation. *Electronics* **2024**, *13*, 1477. [CrossRef]
23. Lee, K.; Back, J.; Choy, I. Nonlinear disturbance observer based robust attitude tracking controller for quadrotor UAVs. *Int. J. Control Autom. Syst.* **2014**, *12*, 1266–1275. [CrossRef]
24. Baraban, G.; Sheckells, M.; Kim, S.; Kobilarov, M. Adaptive Parameter Estimation for Aerial Manipulation. In Proceedings of the American Control Conference, Denver, CO, USA, 1–3 July 2020; pp. 614–619. [CrossRef]
25. Alvarez-Munoz, J.; Marchand, N.; Guerrero-Castellanos, J.F.; Tellez-Guzman, J.J.; Escareno, J.; Rakotondrabe, M. Rotorcraft with a 3DOF Rigid Manipulator: Quaternion-based Modeling and Real-time Control Tolerant to Multi-body Couplings. *Int. J. Autom. Comput.* **2018**, *15*, 547–558. [CrossRef]
26. Park, C.; Ramirez-Serrano, A.; Bisheban, M. Adaptive Incremental Nonlinear Dynamic Inversion Control for Aerial Manipulators. *Aerospace* **2024**, *11*, 671. [CrossRef]
27. Petrlík, M.; Báča, T.; Heřt, D.; Vrba, M.; Krajník, T.; Saska, M. A robust UAV system for operations in a constrained environment. *IEEE Robot. Autom. Lett.* **2020**, *5*, 2169–2176. [CrossRef]
28. Wang, Y.; Lu, Q.; Ren, B. Wind turbine crack inspection using a quadrotor with image motion blur avoided. *IEEE Robot. Autom. Lett.* **2023**, *8*, 1069–1076. [CrossRef]
29. Ullah, S.; Alghamdi, H.; Algethami, A.; Alghamdi, B.; Hafeez, G. Robust Control Design of Under-Actuated Nonlinear Systems: Quadcopter Unmanned Aerial Vehicles with Integral Backstepping Integral Terminal Fractional-Order Sliding Mode. *Fractal Fract.* **2024**, *8*, 412. [CrossRef]
30. Moeini, A.; Lynch, A.F.; Zhao, Q. Exponentially Stable Motion Control for Multirotor UAVs with Rotor Drag and Disturbance Compensation. *J. Intell. Robot. Syst.* **2021**, *103*, 15. [CrossRef]
31. Moeini, A.; Rafique, M.A.; Xue, Z.; Lynch, A.F.; Zhao, Q. Disturbance Observer-Based Integral Backstepping Control for UAVs. In Proceedings of the the International Conference on Unmanned Aircraft Systems (ICUAS), Athens, Greece, 1–4 September 2020; pp. 382–388. [CrossRef]
32. Imran, I.; Wood, K.; Montazeri, A. Adaptive Control of Unmanned Aerial Vehicles with Varying Payload and Full Parametric Uncertainties. *Electronics* **2024**, *13*, 347. [CrossRef]
33. Rafique, M.A. Adaptive Nonlinear Control for Unmanned Aerial Vehicles: Visual Servoing and Aerial Manipulation. Ph.D. Thesis, University of Alberta, Edmonton, AB, Canada, 2022. [CrossRef]
34. Bangura, M. Aerodynamics and Control of Quadrotors. Ph.D. Thesis, College of Engineering and Computer Science, The Australian National University, Canberra, ACT, Canada, 2017.
35. Bouabdallah, S. Design and Control of Quadrotors with Application to Autonomous Flying. Ph.D. Thesis, Ecole Polytechnique Federale de Luasanne, Lausanne, Switzerland, 2007.
36. Khalil, H.K. *Nonlinear Systems*, 3rd ed.; Prentice Hall: Upper Saddle River, NJ, USA, 2002.
37. Bisgaard, M.; la Cour-Harbo, A.; Dimon Bendtsen, J. Adaptive control system for autonomous helicopter slung load operations. *Control Eng. Pract.* **2010**, *18*, 800–811. [CrossRef]
38. Huber, F.; Kondak, K.; Krieger, K.; Sommer, D.; Schwarzbach, M.; Laiacker, M.; Kossyk, I.; Parusel, S.; Haddadin, S.; Albu-Schäffer, A. First analysis and experiments in aerial manipulation using fully actuated redundant robot arm. In Proceedings of the IEEE/RSJ International Conference on Intelligent Robots and Systems (IROS), Tokyo, Japan, 3–7 November 2013; pp. 3452–3457. [CrossRef]
39. Meier, L.; Honegger, D.; Pollefeys, M. PX4: A node-based multithreaded open source robotics framework for deeply embedded platforms. In Proceedings of the IEEE International Conference on Robotics and Automation (ICRA), Seattle, WA, USA, 26–30 May 2015; pp. 6235–6240. [CrossRef]

40. Jiang, Z.; Yu, Y.; Lynch, A. Nonlinear Motion Control of a Multirotor Slung Load System: Experimental Results. In Proceedings of the American Control Conference, Toronto, ON, Canada, 10–12 July 2024; pp. 2851–2857. [CrossRef]
41. Lawati, M.A.; Zhang, Z.; Yan, E.; Lynch, A.F. Nonlinear Control of a Multi-Drone Slung Load System. In Proceedings of the American Control Conference, Denver, CO, USA, 8–10 July 2025; pp. 1989–1996.

Disclaimer/Publisher's Note: The statements, opinions and data contained in all publications are solely those of the individual author(s) and contributor(s) and not of MDPI and/or the editor(s). MDPI and/or the editor(s) disclaim responsibility for any injury to people or property resulting from any ideas, methods, instructions or products referred to in the content.